Applied Surface Science 288 (2014) 579–583

Contents lists available at ScienceDirect

Applied Surface Science

journal homepage: www.elsevier.com/locate/apsusc

Superhydrophobic PDMS surfaces with three-dimensional (3D) pattern-dependent controllable adhesion

Jiale Yong, Qing Yang, Feng Chen*, Dongshi Zhang, Guangqing Du, Hao Bian, Jinhai Si, Feng Yun, Xun Hou

State Key Laboratory for Manufacturing System Engineering & Key Laboratory of Photonics Technology for Information of Shaanxi Province, School of Electronics & Information Engineering, Xi'an Jiaotong University, Xi'an 710049, PR China

ARTICLE INFO

Article history:
Received 17 June 2013
Received in revised form 10 October 2013
Accepted 13 October 2013
Available online 23 October 2013

Keywords:
Superhydrophobicity
Controllable adhesion
3D patterns
Contact modes

ABSTRACT

In this paper, we demonstrate an effective approach for the three-dimensional (3D) pattern-structured superhydrophobic PDMS surfaces with controllable adhesion by using femtosecond laser etching method. By combining different laser power with a multi-layered etching way, various 3D patterns can be fabricated (for example, convex triangle array, round pit array, cylindrical array, convex rhombus array and concave triangle-cone array). The as-prepared surfaces with 3D patterns show superhydrophobic character and water controllable adhesion that range from ultralow to ultrahigh by designing different 3D patterns, on which the sliding angle can be controlled from 1° to 90° (the water droplet is firmly pinned on the superhydrophobic surface without any movement at any tilted angles). The 3D pattern-dependent adhesive property is attributed to the different contact modes. This work will provide a facile and promising strategy for the adhesion adjustment on superhydrophobic surfaces.

1. Introduction

Superhydrophobic surfaces with a water contact angle (CA) higher than 150° have received considerable attention due to their importance in both fundamental research and practical application [1–5]. Nature has illustrated a wide variety of superhydrophobic surfaces with low or high water adhesion. The lotus leaf, with an ultrahigh CA but ultralow water adhesion, is demonstrated as the ideal water-repellent superhydrophobic surface and shows excellent self-cleaning property [6–8]. Many efforts have been made in developing an artificial superhydrophobic surface by mimicking the lotus leaf structure [9–11]. Contrary to this characteristic a new kind of sticky superhydrophobic surface with high water adhesion like rose petal has recently been reported [12]. On this surface, the CA of the water droplet is usually above 150°, while the water droplet would be stuck and would not roll off even with the surface vertical or upside down. The high-adhesion superhydrophobic surfaces can provide some fascinating applications in no loss microdroplet transportation [13–15]. Currently, intense interest has been focused on the multifunctional superhydrophobic surfaces exhibiting controllable adhesive forces and sliding angles (SAs) [1–4]. The controllable adhesion allows the manipulation of water droplets on superhydrophobic surfaces. The surfaces are expected to have particular applications in open microdroplet devices, such as biochemical separation, transport of microdroplets, tissue engineering and microfluidic chips [16–18].

In recent years, micromachining for fabricating superhydrophobic surfaces by a femtosecond laser has attracted much interest because it can not only produce the topography with two scale roughness via a one-step process, but can also be applied to a wide variety of materials [19–24]. Controlled by a computer numerical control system, complex structures can be realized, exhibiting unique wetting property. In our previous investigation, we fabricated a new superhydrophobic surface with hierarchical mesh-porous structure by a femtosecond laser on silicon in ambient environment [25]. The surface showed ultralow water adhesion. On this basis, the surfaces composing of periodic hydrophobic patterns (triangle, circle, and rhombus) were fabricated by femtosecond laser irradiation, exhibiting controllable adhesion [26–28]. However, those surfaces are in fact two-dimension (2D) patterns. For most conventional applications, the 3D pattern-dependent superhydrophobic surfaces have greater significance in practical applications than the 2D pattern-dependent superhydrophobic surfaces, especially in tissue engineering and microfluidic chips [16–18,29]. More versatile and simple ways to fabricate 3D patterned superhydrophobic surfaces with controllable adhesion are still lacking.

In this paper, we demonstrate that the femtosecond laser etching is an effective approach to fabricate 3D pattern-structured superhydrophobic surfaces with controllable adhesion. By

* Corresponding author. Tel.: +86 29 82668420.
E-mail address: chenfeng@mail.xjtu.edu.cn (F. Chen).

0169-4332/$ – see front matter © 2013 Elsevier B.V. All rights reserved.
http://dx.doi.org/10.1016/j.apsusc.2013.10.076

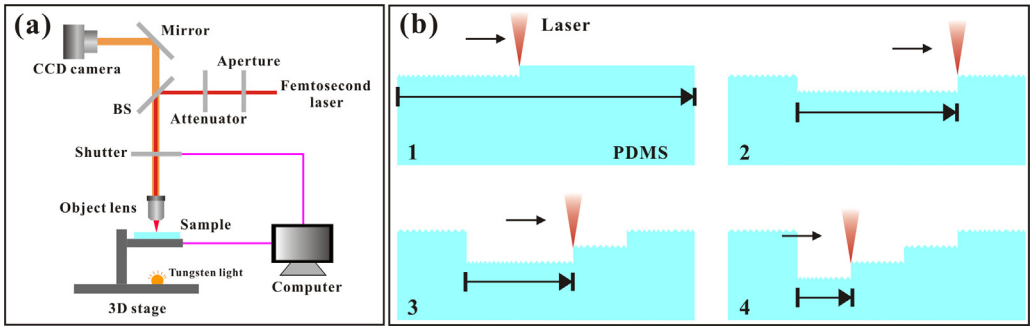

Fig. 1. (a) Schematic of experimental setup. (b) Schematic illustration of the fabrication process of a step structure with three steps.

combining different laser power with a multi-layered etching way, various 3D patterns can be fabricated. The as-prepared surfaces show an analogous superhydrophobicity but high contrast water adhesion that ranges from ultralow to ultrahigh.

2. Experimental section

2.1. Material

Polydimethylsiloxane (PDMS) is an intrinsic hydrophobic material, which has many advantages to be widely applied in tissue engineering and microfluidic chips, such as biocompatibility, thermal stability, nontoxicity and flexibility. In the current investigation, the PDMS thin films were generally prepared from a 10:1 mixture (by weight) of prepolymer (DC-184A, Dow Corning Corporation) and curing agent (DC-184B, Dow Corning Corporation), poured onto the clean glass plates and kept there for 10 min in a vacuum desiccator, so that the trapped air bubbles could emerge to the surface. After removing all the air bubbles, the mixture was solidified in an oven at 100 °C for 2 h. The solidified PDMS samples were carefully peeled off from the glass plate, and then rinsed with deionized water with sonication.

2.2. Surface laser irradiation

The schematic of experiment setup is shown in Fig. 1a. The PDMS samples were mounted on a motorized *x–y–z* translation stage controlled by a computer and positioned perpendicularly to the direction of laser incidence, and then irradiated by a regenerative amplified Ti:sapphire laser system (center wavelength: 800 nm; pulse duration: 50 fs; repetition: 1 kHz). The Gaussian laser beam was focused by a microscope objective lens (10×, NA = 0.30, Nikon) on the front side of the sample. The pulse energy was adjusted by a neutral density attenuator. A mechanical shutter was used as a switch to turn on and off the laser beam. In the experiment, a line-by-line and serial scanning process was used. Each sample was fabricated at a scanning speed of 4 mm/s, and the interval of adjacent laser scanning lines was held constant at 4 μm. At first, the flat PDMS film was entirely serial scanned by femtosecond laser once, leading a layer of hierarchical rough structure (step 1 in Fig. 1b); and then the specified position was only irradiated by a multi-layered etching process (steps 2–4 in Fig. 1b). Therefore, the specified irradiated position could be lower than the prior surface and formed a lowland. The depth of the lowland increased though repeatedly scanning the specified position. The repeatedly irradiated position and the rest section shaped a 3D pattern. As an example, Fig. 1b shows the fabrication process of a step structure with three steps. Following the irradiation process, the samples were cleaned by acetone, alcohol, deionized water in ultrasonic bath at room temperature for 10 min each time.

2.3. Morphology analysis and contact angle characterization

The morphology of the as-prepared surfaces irradiated by a femtosecond laser was observed by a JSM-7000F scanning electron microscopy (SEM, JEOL, Japan). The 3D profile of the fabricated patterns was characterized by a LEXT-OLS4000 laser confocal microscopy (Olympus, Japan). The water CAs and the SAs of 7 μl water droplets on the surfaces ware measured by a JC2000D4 contact-angle system (POWEREACH, China) at ambient temperature, using a sessile drop method.

3. Results and discussion

Fig. 2 shows the SEM images of the structured surface which was scanned by a femtosecond laser once. The surface is characterized by an irregular three-dimensional rough structure of an order of micrometer decorating with tens or hundreds of nm nanostructures. The micro/nanometer binary structures can trap a large amount of air, which is helpful to give rise to superhydrophobicity. The inset in Fig. 2 shows the image of a 7 μl water droplet lying on the laser-induced surface. The static CA on the as-prepared surface

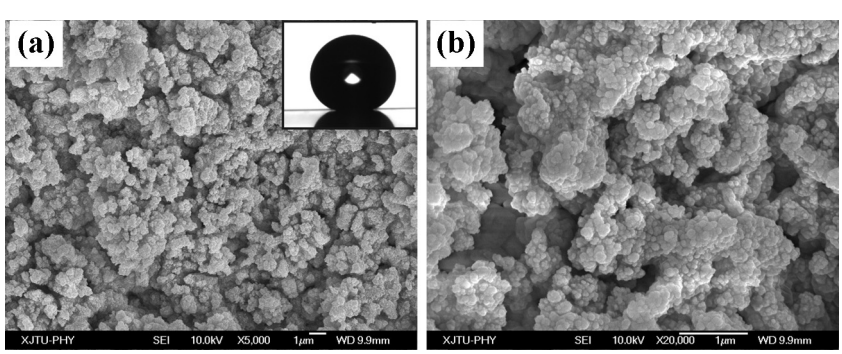

Fig. 2. SEM images of the surface irradiated by a femtosecond laser once. Inset: the shape of a 7 μl water droplet on the as-prepared surface with a contact angle of 157 ± 0.5°.

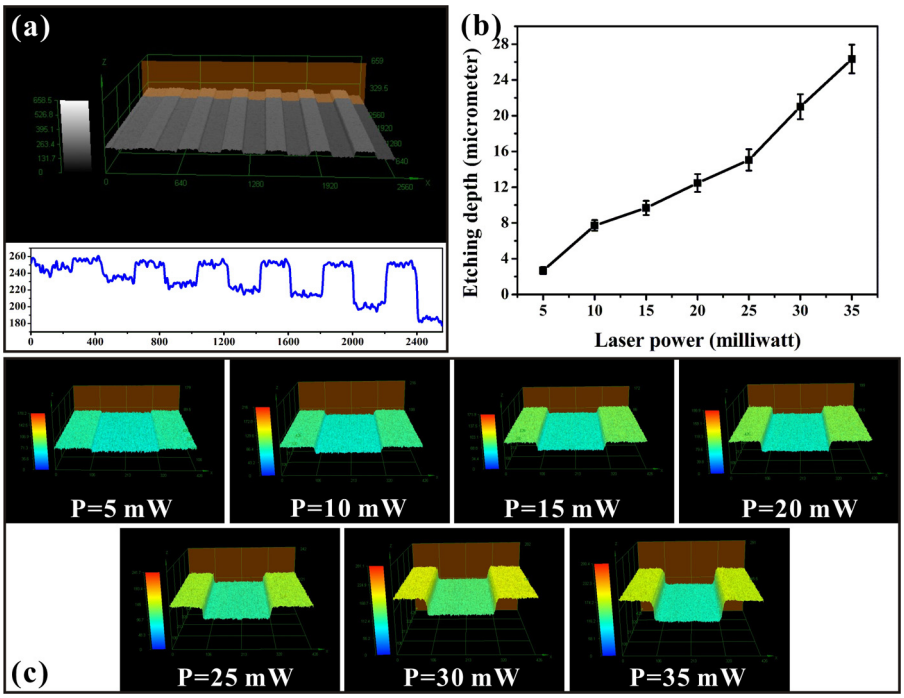

Fig. 3. Dependence of the etching depth on the laser power. (a) 3D image and cross-sectional profile of a series of deep channels fabricated at laser power of 5, 10, 15, 20, 25, 30, 35 mW, respectively. The units for the *x*-, *y*- and *z*-axis are μm. (b) Changing curve of etching depth with the laser power. (c) Magnifying 3D images of deep channels fabricated at different laser power.

is as high as 157° ± 0.5°, even without any modification by materials of low surface energy. Whereas, the SA is lower than 1° (Supporting information, Movie S1), indicating that the water droplet can move very easily even when the surface is only slightly tilted or shaken. Both the high CA and the low SA demonstrate that the laser-induced structure has outstanding character of superhydrophobicity and the dual-scale hierarchical structure is very important to enhance the water repellency of the hydrophobic materials. According to our processing method, there is no a place without laser irradiation. Hence, the finally as-prepared 3D patterns are covered by a hierarchical rough structure and show high CAs.

The laser power, which is the most crucial process parameter, has an important effect on the etching depth. As shown in Fig. 3a, a series of deep channels are fabricated at laser power of 5, 10, 15, 20, 25, 30, 35 mW (from left to right), respectively. It can be found that the etching depth is closely related to the laser

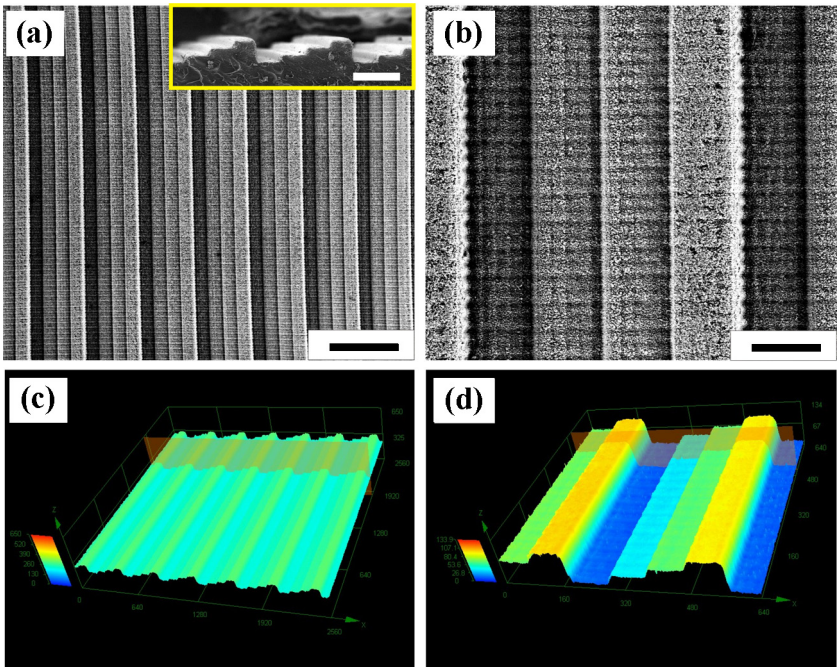

Fig. 4. A step structure fabricated by a multi-layered etching way. (a,b) SEM images of the fabricated step structure. The scale bar represents 500 μm and 100 μm, respectively. The inset shows the cross-sectional SEM image of the step structure (the scale bar is 200 μm). (c,d) 3D images and of the as-prepared surfaces.

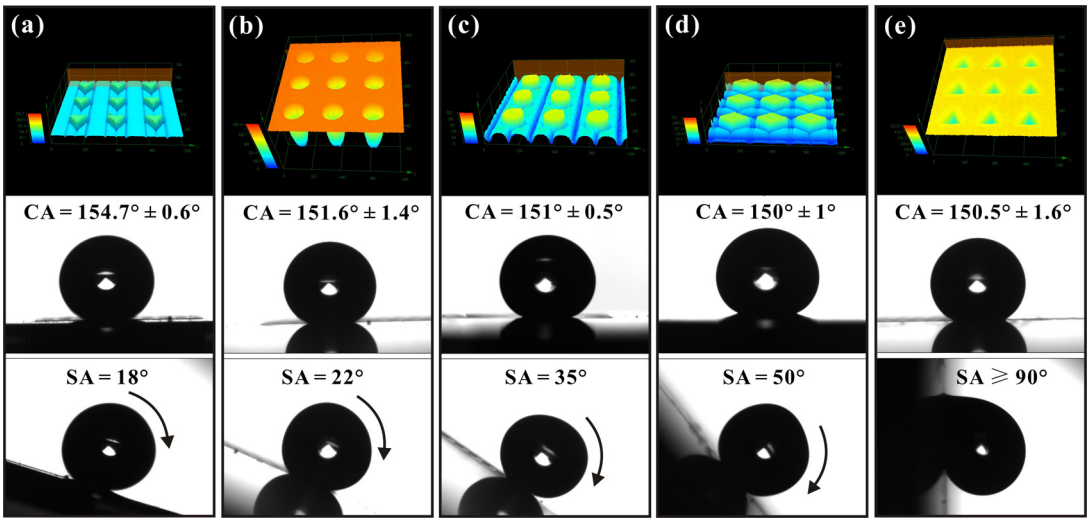

Fig. 5. 3D images, static properties and dynamic behaviors of the different as-prepared 3D pattern-surfaces, respectively. (a) Convex triangle array, (b) round pit array, (c) cylindrical array, (d) convex rhombus array, and (e) concave triangle-cone array.

power and the values increase with the increase of the laser power (Fig. 3b,c). The results agree well with the fact that the higher laser power leads to a more violent ablation process. Interestingly, the etching depth is almost linear with the laser power. Therefore, continuous processing depth can be achieved using different laser power.

A larger etching depth can be achieved by a multi-layered etching way. Fig. 4 shows a step structure with three steps. Every step is rough enough and shows superhydrophobicity (Fig. 4a,b). Fig. 4c,d is the 3D images of the as-prepared surfaces, showing good uniformity of the step structure. In practically, the heights of each step are nearly equal, demonstrating a linear relationship between the etching depth and scanning number of plies. This result implies that the etching depth can be accurately increased by increasing scanning number of plies. Therefore, multi-layered etching makes it possible to fabricate a variety of 3D patterns which exhibit unique wetting properties.

The surfaces with different 3D patterns give rise to different water adhesion which can be shown intuitively in the form of SA. As some examples, Fig. 5 shows 3D topography and wettability of the laser-induced convex triangle array, round pit array, cylindrical array, convex rhombus array and concave triangle-cone array, respectively. The entire as-prepared surfaces are irradiated at a laser power of 30 mW. The five types of 3D patterns all exhibit the superhydrophobic feature (the static CA is 154.7 ± 0.6, 151.6 ± 1.4, 151 ± 0.5, 150 ± 1 and $150.5 \pm 1.6^\circ$, respectively) but high contrast water adhesion. As shown in downmost row of Fig. 5, the SAs on the as-prepared superhydrophobic surfaces are 18, 22, 35, 50 and 90° (the water droplet is firmly pined on the superhydrophobic surface without any movement at any tilted angles) for convex triangle array, round pit array, cylindrical array, convex rhombus array and concave triangle-cone array, respectively (Supporting information, Movies S2–S6). Because all of the surfaces are made of PDMS and treated without additional chemical coating in this study, the modulation of the adhesion of these films is ascribed to the change in surface topography and 3D patterns of PDMS films.

The entire laser-induced surface (non-pattern surface) and above five 3D patterned superhydrophobic PDMS surfaces exhibit different SAs of 1, 18, 22, 35, 50 and 90°, respectively, showing a controllable water adhesion. The difference in adhesion of the as-prepared surfaces is ascribed to the distinct contact modes [30–35]. In the Wenzel state (Fig. 6a), a water droplet can wet the contact area completely. Thus, the water droplet pins the rough surface, and as a result, ultrahigh water adhesion is observed. In contrast, in the Cassie state (Fig. 6b), a water droplet is suspended by the gas layer trapped at the micro- and nanoscale structures. The contact area between the surface and the droplet is so small that the droplet almost has no wetting of the space between the rough structures. Therefore, the adhesion of the surface is extremely low and the water droplet easily rolls off with the surface slightly tilted. However, in most cases, there often exists a transitional state from the Wenzel to the Cassie states, being called Metastable state (Fig. 6c). Water droplets may partially wet the rough surfaces with air trapped in the valleys and slide when the surface is tilted at a certain angle. For example, the entire laser-induced surface (non-pattern surface) showing ultralow adhesion belongs to Wenzel state; concave triangle-cone array showing ultrahigh adhesion belongs to Cassie state; the laser-induced convex triangle array, round pit array, cylindrical array, convex rhombus array showing ordinary adhesion belong to Metastable state. The superhydrophobic state can be artificially tuned from the Wenzel state with high adhesion to the Cassie state with low adhesion through the design of diverse microstructures or patterns to control certain solid/liquid contact modes. In our method, by designing different 3D patterns, the water adhesion on the superhydrophobic surface can be tuned successfully.

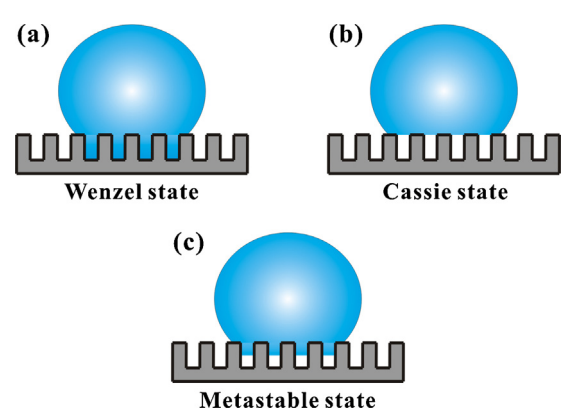

Fig. 6. Schematic illustration of the different contact modes: (a) Wenzel state, (b) Cassie state, and (c) Metastable state.

4. Conclusions

In conclusion, an effective approach to realize controllable adhesive superhydrophobic surfaces with 3D patterns by a femtosecond laser etching method is demonstrated. By designing different 3D patterns, the adhesion of the as-prepared surfaces can be controlled from ultralow to ultrahigh. This 3D pattern-dependent adhesive property is attributed to the different contact modes. The superhydrophobic PDMS surfaces with 3D pattern structures showing controllable adhesion have important potential applications in bioengineering and microfluidic chips.

Acknowledgments

This work is supported by the National Science Foundation of China under the Grant Nos. 61275008 and 61176113, the Special-funded program on National Key Scientific Instruments and Equipment Development of China under the Grant No. 2012YQ12004706 and the Fundamental Research Funds for the Central Universities.

Appendix A. Supplementary data

Supplementary data associated with this article can be found, in the online version, at http://dx.doi.org/10.1016/j.apsusc.2013.10.076.

References

[1] X. Yao, Y.L. Song, L. Jiang, Advanced Materials 23 (2011) 719–734.
[2] T. Verho, C. Bower, P. Andrew, S. Franssila, O. Ikkala, R.H.A. Ras, Advanced Materials 23 (2011) 673–678.
[3] X.M. Li, D. Reinhoudt, M.C. Calama, Chemical Society Reviews 36 (2007) 1350–1368.
[4] W. Song, D.D. Veiga, C.A. Custodio, J.F. Mano, Advanced Materials 21 (2009) 1830–1834.
[5] Z. Wang, C. Lopez, A. Hirsa, N. Koratkar, Applied Physics Letters 91 (2007) 023105.
[6] W. Barthlott, C. Neinhuis, Planta 202 (1997) 1–8.
[7] V. Zorba, E. Stratakis, M. Barberoglou, E. Spanakis, P. Tzanetakis, S.H. Anastasiadis, C. Fotakis, Advanced Materials 20 (2008) 4049–4095.
[8] M. Barberoglou, V. Zorba, E. Stratakis, E. Spanakis, P. Tzanetakis, S.H. Anastasiadis, C. Fotakis, Applied Surface Science 255 (2009) 5425–5429.
[9] F. Xia, L. Jiang, Advanced Materials 20 (2008) 2842–2858.
[10] Y.B. Zhang, Y. Chen, L. Shi, J. Li, Z.G. Gao, Journal of Materials of Chemistry 22 (2012) 799–815.
[11] Y.L. Zhang, Q.D. Chen, Z. Jin, E. Kim, H.B. Sun, Nanoscale 4 (2012) 4858–4869.
[12] L. Feng, Y.N. Zhang, J.M. Xi, Y. Zhu, N. Wang, F. Xia, L. Jiang, Langmuir 24 (2008) 4114–4119.
[13] M.H. Jin, X.J. Feng, L. Feng, T.L. Sun, J. Zhai, T.J. Li, L. Jiang, Advanced Materials 17 (2005) 1977–1981.
[14] M. Wang, C. Chen, J.P. Ma, J. Xu, Journal of Materials Chemistry 21 (2011) 6962–6967.
[15] D. Wu, S.Z. Wu, Q.D. Chen, Y.L. Zhang, J. Yao, X. Yao, L.G. Niu, J.N. Wang, L. Jiang, H.B. Sun, Advanced Materials 23 (2011) 545–549.
[16] Y.L. Zhang, H. Xia, E. Kim, H.B. Sun, Soft Matter 8 (2012) 11217–11231.
[17] K.S. Liu, L. Jiang, Annual Review of Materials Research 42 (2012) 231–263.
[18] K.S. Liu, L. Jaing, Nano Today 6 (2011) 155–175.
[19] J.L. Yong, F. Chen, Q. Yang, D.S. Zhang, H. Bian, G.Q. Du, J.H. Si, X.W. Meng, X. Hou, Langmuir 29 (2013) 3274–3279.
[20] X.H. Wang, F. Chen, H.W. Liu, W.W. Liang, Q. Yang, J.H. Si, X. Hou, Optics Communications 284 (2011) 317–321.
[21] J. Bonse, K.W. Brzeinka, A.J. Meixner, Applied Surface Science 221 (2004) 215–230.
[22] J. Bonse, S. Bandach, J. Kruger, W. Kautek, M. Lenzer, Applied Physics A 74 (2002) 19–25.
[23] M. Zhou, H.F. Yang, B.J. Dai, J.K. Di, E.L. Zhao, L. Cai, Applied Physics A 94 (2009) 571–576.
[24] J.L. Yong, F. Chen, Q. Yang, G.Q. Du, H. Bian, D.S. Zhang, J.H. Si, F. Yun, X. Hou, ACS Applied Materials & Interfaces 5 (2013) 9382–9385, http://dx.doi.org/10.1021/am402923t.
[25] J.L. Yong, Q. Yang, F. Chen, D.S. Zhang, H. Bian, Y. Ou, J.H. Si, G.Q. Du, X. Hou, Applied Physics A 111 (2013) 243–249.
[26] D.S. Zhang, F. Chen, Q. Yang, J.L. Yong, H. Bian, Y. Ou, J.H. Si, X.W. Meng, X. Hou, ACS Applied Materials & Interfaces 4 (2012) 4905–4912.
[27] F. Chen, D.S. Zhang, Q. Yang, X.H. Wang, B.J. Dai, X.M. Li, X.Q. Hao, Y.C. Ding, J.H. Si, X. Hou, Langmuir 27 (2011) 359–436.
[28] D.S. Zhang, F. Chen, Q. Yang, J.H. Si, X. Hou, Soft Matter 7 (2011) 8337–8342.
[29] A. Pruna, J. Ramiro, L. Belforte, Journal of Physics and Chemistry of Solids 74 (2013) 1640–1645.
[30] S.T. Wang, L. Jiang, Advanced Materials 19 (2007) 3423–3424.
[31] Y.M. Zheng, X.F. Gao, L. Jiang, Soft Matter 3 (2007) 178–182.
[32] J. Li, X.H. Liu, Y.P. Ye, H.D. Zhou, J.M. Chen, The Journal of Physical Chemistry C 115 (2011) 4726–4729.
[33] Q.B. Zhang, J. Wang, Materials Letters 67 (2012) 334–337.
[34] C.B. Ran, G.Q. Ding, W.C. Liu, Y. Deng, W.T. Hou, Langmuir 24 (2008) 9952–9955.
[35] K.Q. Li, X.R. Zeng, H.Q. Li, X.J. Lai, C.X. Ye, H. Xie, Applied Surface Science 279 (2013) 458–463.